A method for accelerating the molecular dynamics simulation of infrequent events

Arthur F. Voter
Theoretical Division, Los Alamos National Laboratory, Los Alamos, New Mexico 87545

(Received 24 June 1996; accepted 10 December 1996)

For infrequent-event systems, transition state theory (TST) is a powerful approach for overcoming the time scale limitations of the molecular dynamics (MD) simulation method, provided one knows the locations of the potential-energy basins (states) and the TST dividing surfaces (or the saddle points) between them. Often, however, the states to which the system will evolve are not known in advance. We present a new, TST-based method for extending the MD time scale that does not require advanced knowledge of the states of the system or the transition states that separate them. The potential is augmented by a bias potential, designed to raise the energy in regions *other* than at the dividing surfaces. State to state evolution on the biased potential occurs in the proper sequence, but at an accelerated rate with a nonlinear time scale. Time is no longer an independent variable, but becomes a statistically estimated property that converges to the exact result at long times. The long-time dynamical behavior is exact if there are no TST-violating correlated dynamical events, and appears to be a good approximation even when this condition is not met. We show that for strongly coupled (i.e., solid state) systems, appropriate bias potentials can be constructed from properties of the Hessian matrix. This new ''hyper-MD'' method is demonstrated on two model potentials and for the diffusion of a Ni atom on a Ni(100) terrace for a duration of 20 μs. © *1997 American Institute of Physics.* [S0021-9606(97)50211-X]

I. INTRODUCTION

The molecular dynamics (MD) simulation method is a powerful and widely used tool. A long-standing problem, however, is that its utility is limited to processes that occur on a time scale of nanoseconds or less. While recent innovations in parallel computing hardware have dramatically increased the number of atoms that can be simulated, they have had little impact on the time scales accessible to MD, due to the sequential nature of the integration of the equations of motion. Consequently, many processes of interest remain out of reach.

For many systems, the dynamics can be characterized as a sequence of infrequent transitions from one potential basin (''state'') to another. In these cases, longer time scales can be accessed using transition state theory (TST), an elegant approach with a long history.[1–6] In TST, one takes the transition rate between states as the flux through a dividing surface separating the states. This flux is an equilibrium property of the system, and so does not require that actual dynamics be performed. TST assumes that each crossing of the dividing surface corresponds to a true reactive event, in which the system passes from one state to another and then loses all memory of this transition before the next event. In actuality, some surface crossings can be dynamically connected, i.e., if the time between two successive crossings does not exceed the correlation time of the system. Because of this correlated dynamical behavior the TST rate constant is only approximate, but the exact rate can be recovered by computing a dynamical correction factor from short-duration trajectories initiated at the dividing surface,[7–9] as first demonstrated by Keck[10] in the gas phase and Bennett[11] for condensed phase systems. If the TST dividing surface is chosen carefully, so as to minimize these correlated dynamical effects (e.g., by placing it at the saddle surface), the TST rate constant is often an extremely good approximation to the true rate for strongly coupled (e.g., solid state) systems. This fact, along with the conceptual simplicity and accuracy of the harmonic approximation to TST,[12] has led to the widespread use of TST for problems in the solid state. Properly applied, the errors due to the harmonic approximation and any missing correlated dynamics are usually substantially smaller than the errors associated with the approximate interatomic potential. The dynamical evolution of infrequent-event systems can thus be viewed, justifiably, as a sequence of uncorrelated passages from state to state via saddle points on the potential surface.

However, the utility of TST in treating infrequent-event dynamics has always rested on two crucial assumptions; that one knows in advance what the different states of the system will be, and that one can construct reasonable dividing surfaces along the boundaries between these states, or can find saddle points. Often, however, the understanding of the states to which a system will evolve is incomplete. Indeed, determining the future configurations may be the primary motivation for the atomistic simulation. Perhaps worse, presumptions about how the system will evolve may be incorrect, so that important pathways are overlooked. For example, the substrate-exchange mechanism for adatom diffusion on fcc(100) surfaces, which was unknown (and unexpected) until 1990,[14] is now understood to be the dominant surface transport mechanism for some transition metals.[15,16] This has forced a re-examination of models of surface dynamics based on simple hopping events. Other, more complicated events can also occur on surfaces, involving the con-

certed motion of dozens of atoms.[17] Their unexpected and complex nature virtually guarantees they will be omitted from lattice-based, kinetic Monte Carlo simulations, which are typically based (implicitly or explicitly) on a catalog of TST rate constants.[18]

In this paper we take a new approach to the infrequent-event problem. We present a method for extending the time scale of a molecular dynamics simulation without any advanced knowledge of either the dividing surfaces or the states through which the system may evolve. First, appealing to the general TST expression, we show that it is possible to modify the potential energy surface in such a way that a molecular dynamics simulation on this modified surface exhibits the correct relative probabilities for escape from any state of the system to the various adjacent states, but with enhanced overall escape rates. The time scale for the evolution of the system can only be known in a coarse-grained sense, but a statistical estimate of the elapsed time is easily accumulated as the simulation evolves. The long-time dynamics in this type of simulation are exact to the extent that the dynamical corrections to TST are negligible. We then show that the requirement on the modified potential, that it match the original potential at the TST dividing surfaces, can be met to a good approximation using only local properties of the Hessian matrix, with no advance knowledge of the states in the system. In Sec. III A, we investigate the properties of this ''hyper-MD'' method for one-dimensional diffusion of a particle in a simple two-dimensional potential. The viability of the method for more complex, realistic systems is then demonstrated in Sec. III B in a simulation of adatom diffusion on a small Ni(100) terrace for tens of microseconds, a time scale that is generally inaccessible using direct MD on present-day computers.

The hyper-MD method should be most appropriate for processes in the solid state, where atoms are strongly coupled together. Examples include surface and bulk diffusion, overlayer growth, annealing of ion-implant damage, and low-strain-rate propagation of a crack tip. In its present form, it is not suitable for accelerating dynamics in the liquid phase. First is the assumption that TST is a good approximation, which is often not the case for reactions in solution.[19] Second, the existence of negative eigenvalues of the Hessian, typically abundant in the liquid state, obscure the identification of the saddle points for the reaction coordinate. For these same reasons, the method may not be useful for solid state systems with significantly floppy modes, such as for certain molecular adsorbates.

This method compliments other recently developed approaches[20–23] for extending the atomistic simulation time scale, and might be usefully combined with them. For systems with a natural disparity in vibrational frequencies, Tuckerman, Martyna, and Berne[24] have developed a multiple-time-step integration algorithm, and Grønbech-Jensen and Doniach[20] and Mathiowetz *et al.*[21] have presented methods for accelerating protein-folding dynamics by eliminating the fast vibrational modes completely.

II. THEORY

A. Accelerated dynamics in a biased potential

Consider a system of N atoms, evolving according to the classical equations of motion, characterized at any time t by $\mathbf{r}(t)$ and $\mathbf{p}(t)$, the $3N$-dimensional vectors for the atom positions and momenta, respectively. The system resides initially in a basin of the potential energy function, $V(\mathbf{r})$, that we will call state A. In the transition state theory (TST) approximation, the unimolecular rate constant for escape from this state[25] is given by the flux exiting through the boundary to state A (the $3N-1$-dimensional surface that separates state A from other states),

$$k_{A\rightarrow}^{\mathrm{TST}}=\langle|v_A|\,\delta_A(\mathbf{r})\rangle_A\,. \tag{1}$$

Here $\delta_A(\mathbf{r})$ is a Dirac delta function positioned at the boundary to state A and v_A is the velocity normal to this boundary surface. These are defined via $F_A(\mathbf{r})$, a continuous, differentiable function chosen to have the property

$$F_A(\mathbf{r})\begin{cases}>0 & \text{if } \mathbf{r} \text{ is in state } A\\ =0 & \text{if } \mathbf{r} \text{ is on the boundary to state } A\\ <0 & \text{if } \mathbf{r} \text{ is outside of state } A.\end{cases} \tag{2}$$

The occupation function

$$\Theta_A(\mathbf{r})\equiv\theta[F(\mathbf{r})] \tag{3}$$

is unity when the system is in state A, and zero otherwise (θ is the standard step function, while occupation functions will be indicated by capital Θ), so that its spatial derivative gives the desired delta function,

$$\delta_A(\mathbf{r})\equiv\nabla\Theta_A(\mathbf{r})=\delta[F_A(\mathbf{r})]|\nabla F_A(\mathbf{r})|, \tag{4}$$

and the normal velocity is

$$v_A=-\frac{\nabla F_A\cdot\dot{\mathbf{r}}}{|\nabla F_A|}, \tag{5}$$

where $\dot{\mathbf{r}}=d\mathbf{r}/dt$. We will only consider the canonical ensemble, for which averages such as in Eq. (1) are defined by the usual ratio of $6N$-dimensional phase-space integrals,

$$\langle P\rangle\equiv\frac{\int\int P(\mathbf{r},\mathbf{p})e^{-\beta K(\mathbf{p})}e^{-\beta V(\mathbf{r})}d\mathbf{r}d\mathbf{p}}{\int\int e^{-\beta K(\mathbf{p})}e^{-\beta V(\mathbf{r})}d\mathbf{r}d\mathbf{p}}. \tag{6}$$

Here $\beta=1/k_BT$ (k_B is the Boltzmann constant and T is the temperature) and $K(\mathbf{p})$ is the kinetic energy ($\Sigma_i^{3N}p_i^2/2m_i$), where m_i is the mass of the atom associated with coordinate i. The subscript A on the average in Eq. (1) indicates restriction to the configuration space of state $A[\langle P\rangle_A\equiv\langle P\Theta_A(\mathbf{r})\rangle]$. We note that $\Theta_A(\mathbf{r})$ cuts $\delta_A(\mathbf{r})$ in half, eliminating the factor of 1/2 that sometimes appears in the definition of k^{TST} to account for outgoing flux only.

Because the kinetic energy is separable, the momentum dependence in Eq. (1) can be integrated out analytically if the effective mass of the reaction coordinate is constant over the TST surface (i.e., if the surface is planar or all the atomic masses are equivalent). In the present treatment, we keep the full phase-space average to allow for arbitrarily curved TST

surfaces,[26] and to allow for the possibility of a surface definition that depends on both **r** and **p**, although we only consider **r**-based definitions.

Now consider adding to $V(\mathbf{r})$ a continuous, non-negative bias (or ''boost'') potential, $\Delta V_b(\mathbf{r})$, designed so that $\Delta V_b(\mathbf{r})=0$ where $\delta_A(\mathbf{r})\neq 0$, i.e., the potential is unaffected at the transition state region. A schematic example is shown in Fig. 1. Deferring until Sec. II B the discussion of how to construct $\Delta V_b(\mathbf{r})$, we manipulate Eq. (1) to obtain

$$k_{A\rightarrow}^{\mathrm{TST}}=\frac{\int\int|v_A|\,\delta_A(\mathbf{r})\Theta_A(\mathbf{r})e^{-\beta K(\mathbf{p})}e^{-\beta V(\mathbf{r})}d\mathbf{r}d\mathbf{p}}{\int\int e^{-\beta K(\mathbf{p})}e^{-\beta V(\mathbf{r})}d\mathbf{r}d\mathbf{p}}$$

$$=\frac{\int\int|v_A|\,\delta_A(\mathbf{r})\Theta_A(\mathbf{r})e^{-\beta K(\mathbf{p})}e^{-\beta[V(\mathbf{r})+\Delta V_b(\mathbf{r})]}e^{+\beta\Delta V_b(\mathbf{r})}d\mathbf{r}d\mathbf{p}}{\int\int e^{-\beta K(\mathbf{p})}e^{-\beta V(\mathbf{r})}d\mathbf{r}d\mathbf{p}}$$

$$=\frac{\langle|v_A|\,\delta_A(\mathbf{r})e^{\beta\Delta V_b(\mathbf{r})}\rangle_{A_b}}{\langle e^{\beta\Delta V_b(\mathbf{r})}\rangle_{A_b}},\tag{7}$$

where the subscript A_b indicates an ensemble average taken on the biased potential surface $V(\mathbf{r})+\Delta V_b(\mathbf{r})$ within state A,

$$\langle P\rangle_{A_b}=\frac{\int\int P(\mathbf{r},\mathbf{p})\Theta_A(\mathbf{r})e^{-\beta K(\mathbf{p})}e^{-\beta[V(\mathbf{r})+\Delta V_b(\mathbf{r})]}d\mathbf{r}d\mathbf{p}}{\int\int e^{-\beta K(\mathbf{p})}e^{-\beta[V(\mathbf{r})+\Delta V_b(\mathbf{r})]}d\mathbf{r}d\mathbf{p}};\tag{8}$$

i.e., we define state A_b as state A with the biasing potential turned on. Because $\Delta V_b(\mathbf{r})=0$ wherever $\delta_A(\mathbf{r})\neq 0$, the numerator in the last line of Eq. (7) simplifies, leaving

$$k_{A\rightarrow}^{\mathrm{TST}}=\frac{\langle|v_A|\,\delta_A(\mathbf{r})\rangle_{A_b}}{\langle e^{\beta\Delta V_b(\mathbf{r})}\rangle_{A_b}}.\tag{9}$$

The numerator in Eq. (9) is simply the TST rate of escape from state A_b, while the denominator is equivalent to the ratio of partition functions for states A and A_b.

The derivation to this point is essentially standard importance sampling.[27–31] Knowing the location of the dividing surface, one can use Eq. (9) to obtain the TST escape rate from state A, an equilibrium property of the system, using either Monte Carlo or MD. We now begin a different tack, exploiting Eq. (9) to formulate a dynamical method that does not depend on knowledge of the dividing surface nor on complete sampling of the reactant state. The primary goal will not be to compute rate constants per se (although in the examples in Sec. III, rates are determined to demonstrate the accuracy and viability of the method), but rather to devise an algorithm that is capable of advancing a system from state to state much more rapidly than is possible with direct MD simulation.

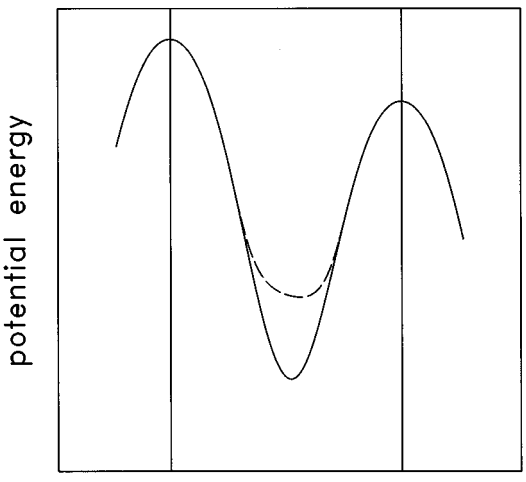

FIG. 1. Schematic illustration of a one-dimensional potential V (solid line) defining state A, and the biased potential $V+\Delta V_b$ (dashed line), which defines state A_b. The potentials are equivalent at the TST boundaries (indicated by vertical lines), so the relative probability of escape to the left vs right is the same for both states, although the escape rates are enhanced for state A_b.

Assume that we have a system for which TST is exact, i.e., any crossing of the TST dividing surface corresponds to a true reactive event and the crossing is not dynamically correlated with any past or future crossing event. Further, assume that modifying $V(\mathbf{r})$ with the bias potential does not affect this lack of dynamical connectivity, so that TST is exact for this biased potential. Finally, assume that $\Delta V_b(\mathbf{r})$ is chosen such that it does not block any escape paths, nor introduce any new, significant wells into the system; i.e., any subminima within state A_b have escape times substantially shorter than the escape time (τ_{esc}^{A}) for state A. We now consider the dynamical properties of the biased-potential system.

The biasing potential enhances the TST escape rate because the A_b well is not as deep as the A well [$\Delta V_b(\mathbf{r})$ is everywhere non-negative]. Also, because $\Delta V_b(\mathbf{r})$ does not affect any part of the TST surface, the ratios of the TST escape rates to each of the states adjacent to state A are preserved. This is because the expression for the TST escape rate to any particular adjacent state (e.g., $k_{A\rightarrow B}^{\mathrm{TST}}$) has as its denominator the partition function for state A. Replacing this denominator with the partition function for state A_b leaves intact the ratio of escape rates to any two different adjacent states (e.g., B and C),

$$\frac{k_{A\rightarrow B}^{\mathrm{TST}}}{k_{A\rightarrow C}^{\mathrm{TST}}}=\frac{k_{A_b\rightarrow B}^{\mathrm{TST}}}{k_{A_b\rightarrow C}^{\mathrm{TST}}}.\tag{10}$$

This is a crucial property, with the consequence that if we run a trajectory[32] on the biased potential surface, we will observe accelerated escape to an appropriate adjacent state, B. Because we have specified that the system obeys TST, this trajectory will thermalize in state B. If, in turn, state B has a biasing potential, the system will again exhibit accelerated escape to a state adjacent to B, and so on. *At an accelerated pace, the system evolves from state to state in a sequence representative of the exact dynamics.* (That is, the probability of any given sequence, e.g., $A-B-A-C-D-E$..., is exactly the same for the biased dynamics as for the exact dynamics.) We now ask whether a time scale can be assigned to this accelerated dynamical evolution. In fact, such a time scale is easy to define, provided that we only require that it be meaningful in a long-time or coarse-grained sense.

Consider a thought experiment in which we evaluate the averages in Eq. (9) using molecular dynamics within state A_b. Rather than using many short, microcanonical trajecto-

ries sampled from the canonical ensemble, we instead use one long trajectory. By coupling this trajectory, at least weakly, to a heat bath (e.g., using one of the modern thermostat methods), we guarantee that over time the proper canonical phase space is sampled. By making the trajectory extremely long, the averages can be computed to arbitrarily high accuracy. A reflecting barrier[33] along the TST dividing surface contains the trajectory within state A_b and provides a count of the the number of TST surface collisions, or escape attempts (n_{esc}). Inverting Eq. (9) gives an expression for the average time required for escape from state A, which is evaluated from the trajectory results as

$$\tau_{\mathrm{esc}}^{A}=\frac{1}{k_{A\rightarrow}^{\mathrm{TST}}}=\frac{\langle e^{\beta\Delta V_b(\mathbf{r})}\rangle_{A_b}}{\langle|v_A|\delta_A(\mathbf{r})\rangle_{A_b}}$$
$$=\frac{\frac{1}{n_{\mathrm{tot}}}\sum_{i=1}^{n_{\mathrm{tot}}}e^{\beta\Delta V_b[\mathbf{r}(t_i)]}}{n_{\mathrm{esc}}/(n_{\mathrm{tot}}\Delta t_{\mathrm{MD}})}$$
$$=\frac{1}{n_{\mathrm{esc}}}\sum_{i=1}^{n_{\mathrm{tot}}}\Delta t_{\mathrm{MD}}e^{\beta\Delta V_b[\mathbf{r}(t_i)]}, \tag{11}$$

where Δt_{MD} is the integration time step, n_{tot} is the total number of MD steps, and t_i indicates the time at the ith MD step. Utilizing the equivalence between an ensemble average and a time average, the numerator has been evaluated using the n_{tot} equal-time snapshots. The denominator, which is the TST escape rate from A_b, has been expressed as the number of TST surface crossings (or, in this case, reflections) divided by the total trajectory time. Our goal is not actually to calculate τ_{esc}^{A}, but rather to discover the time scale of the biased dynamics. Inspection of the last line of Eq. (11) suggests a simple definition for the time evolved per MD step on the biased potential. By requiring that the total time evolved, divided by the number of attempted escapes, equal the average escape time, we arrive at

$$\Delta t_{b_i}=\Delta t_{\mathrm{MD}}e^{\beta\Delta V_b[\mathbf{r}(t_i)]}, \tag{12}$$

where the total (''boosted'') time that the system has evolved is estimated as

$$t_b=\sum_{i}^{n_{\mathrm{tot}}}\Delta t_{b_i}. \tag{13}$$

While this definition is meaningless on short (i.e., vibrational) time scales, it nonetheless allows us to advance the clock at each MD step. The amount the clock is advanced depends on the strength of the bias at the current position of the trajectory. Where the boost potential is zero, $\Delta t_b=\Delta t_{\mathrm{MD}}$, as for normal MD. At long time scales, by construction, the time on this clock converges on the correct result (t_{exact}),

$$\lim_{n_{\mathrm{tot}}\rightarrow\infty}\left(\frac{t_b}{t_{\mathrm{exact}}}\right)=1, \tag{14}$$

because from Eq. (11), which is exact for an infinitely long trajectory, $t_b=\tau_{\mathrm{esc}}^{A}n_{\mathrm{esc}}$. We define the average boost factor (the speed improvement compared to direct MD, ignoring the extra cost of evaluating the bias potential) as

$$\frac{t_b}{t_{\mathrm{MD}}}=\langle e^{\beta\Delta V_b(\mathbf{r})}\rangle=\frac{1}{n_{\mathrm{tot}}}\sum_{i=1}^{n_{\mathrm{tot}}}e^{\beta\Delta V_b[\mathbf{r}(t_i)]}. \tag{15}$$

This accelerated dynamical approach, which we term hyperdynamics or hyper-MD, transforms the problem into one where the dynamical evolution from state to state is correct, but the time scale is distorted, sometimes running too fast and other times too slow, relative to the average accelerated pace. At long times, the many bad estimates of the short-time intervals sum up to an increasingly accurate estimate of the total time. What is a ''long'' time depends on the statistical properties of the time-dependent boost factor, $e^{\beta\Delta V_b[\mathbf{r}(t)]}$. If escape from a state requires a number of MD steps that is large enough to obtain a high-quality estimate of the average boost factor, then the accuracy of individual escape-time predictions will be quite good. This is the case for the examples presented below. In contrast, an aggressive choice for $\Delta V_b(\mathbf{r})$ may stimulate escape in a small number of steps. In this case, the predicted time for a single escape is very noisy, so the time scale becomes meaningful only after many transitions. In either case, the escape time estimates will be unbiased, and the error in a particular escape time will be uncorrelated with the time error of future escapes from other states, even if each state is different. By the central limit theorem, then, the relative error in the estimate of the total time will decrease as $t^{-(1/2)}$.

If $\Delta V_b(\mathbf{r})$ is chosen too aggressively, it may violate the requirements stated above. For example, $\Delta V_b(\mathbf{r})$ might confine the trajectory to a subset of the binding site, so that not all escape paths can be found readily. In an extreme case, a trajectory entering a new state might encounter a repulsive bias potential that causes it to quickly exit through the same region of the TST boundary without sampling the rest of the state. In these cases, the calculation will lose accuracy, because artificial correlations are introduced into the successive TST crossing events. In general, though, there is nothing wrong with a bias potential that raises the energy of parts of the state above the energy of the saddle points, provided that it does not block the ergodic sampling of the entire state.

Assuming that $\Delta V_b(\mathbf{r})$ can be determined purely from local properties of $V(\mathbf{r})$, an important feature of this hyper-MD approach is that it has the ''efficiency'' of a direct-MD simulation. When the system makes a transition from state A to an adjacent state, it does so with the correct probability relative to the other possible transitions out of state A, even though the trajectory never ''sees'' the other possible escape paths (it never sees the other paths because it exits state A through the first escape path it finds). In contrast, the usual approach for accelerating infrequent events involves first finding (or knowing) all the possible escape paths and the rate constant associated with each one, and then picking one escape route that is consistent with the relative probabilities. This perspective underpins any kinetic Monte Carlo simulation and is implicit in a master equation approach. If all the escape paths and associated rate constants

can be estimated quickly for the current state of the system, this rate-based approach is unquestionably superior to the hyper-MD method presented in this paper. However, if the system resides in a state for which the escape paths are unknown, and are perhaps complicated, then one must undertake a search to find each saddle point. Given that the number of saddle points bounding a state will generally be proportional to N, and that finding one saddle point to a certain accuracy requires computational work scaling as N^2, the overall scaling of this rate-based approach becomes N^3 or worse. An attempt to speed up this process by computing approximate barrier heights will give rise to exponential errors that do not necessarily cancel out, in contrast to the time-based hyper-MD.

B. Defining the bias potential

The key to implementing the hyper-MD method is choosing a computationally tractable definition for $\Delta V_b(\mathbf{r})$. As stated above, the requirements on $\Delta V_b(\mathbf{r})$ are that it be zero at all the dividing surfaces, and that it not introduce new subwells with escape times that rival the true escape time from the well. To make the method useful as a general tool, the definition should not depend on advanced knowledge of the states of the system, nor require a search for saddle points. There may be many ways to define such a function; the approach we take is based on local properties of the potential via the $\mathbf{r}$-dependent gradient vector, $\mathbf{g}\{g_i \equiv [\partial V(\mathbf{r})/\partial x_i]\}$, and Hessian matrix, $\mathbf{H}$ $\{H_{ij} \equiv [\partial^2 V(\mathbf{r})/\partial x_i \partial x_j]$, where x_i and x_j are components of the $3N$-dimensional vector $\mathbf{r}\}$.

In essence, the relevant properties of the potential can be described using the usual two-dimensional analogy of the hiker in the mountains. Each valley is a state. To get to the next valley the hiker goes over a mountain pass. The maximum along a minimum-energy pathway to the next state is a first-order saddle point, i.e., $|\mathbf{g}|=0$ and $\mathbf{H}$ has exactly one negative eigenvalue. Considering all the possible ways that the hiker can leave the valley leads one to define the TST boundary as the ridge line surrounding this valley. This ridge line, which includes the first-order saddles, can be characterized as the set of points at which the lowest eigenvalue (ϵ_1) of the Hessian is negative, and that have zero derivative along the direction of the lowest eigenvector ($\mathbf{C}_1$); i.e., these points satisfy

$$\mathbf{C}_1^{\dagger}\mathbf{g}=0 \quad \text{and} \quad \epsilon_1<0. \tag{16}$$

This definition for the TST surface has been proposed by Sevick, Bell, and Theodorou,[34] who give a good discussion of its merits and limitations. At a first-order saddle point, Eq. (16) is ideal, defining the so-called saddle plane, the hyperplane orthogonal to the reaction coordinate at that point. Taking the saddle plane as the global TST surface for a two-state system underpins a full harmonic TST treatment such as the Vineyard method,[12] and is the planar surface that minimizes the recrossing events.[35] Away from a first-order saddle, where Eq. (16) describes a surface that deviates from the saddle plane, the situation is more complicated, especially in many dimensions.

For the $3N$-dimensional system, the general, nonlocal definition of the TST boundary is based on the consequence of a steepest-descent minimization. The basin belonging to state A is defined by the set of points from which a steepest descent path leads to the minimum of state A. This basin is bounded by a $3N$-1-dimensional hypersurface, the TST surface, just outside of which all steepest descent paths lead to states other than A. Near any first-order saddle point, Eq. (16) gives a good approximation to this true TST dividing surface. Further from the saddle, the approximation can break down.[34] For example, $\mathbf{H}$ may have more than one negative eigenvalue, and the reaction coordinate may not correspond to the lowest one. Also, Eq. (16) can be satisfied in regions internal to a state that have nothing to do with a state-to-state boundary. And for some parts of the TST surface, the Hessian may have *no* negative eigenvalues. These considerations imply that it is probably impossible to find a rigorous, local definition for the TST dividing surface.

However, our task is to define a form for $\Delta V_b(\mathbf{r})$ that is zero at the TST surface; this does not require knowing the exact position of the TST surface. Moreover, if we can choose $\Delta V_b(\mathbf{r})$ such that it is zero at the most important parts of the dividing surface (i.e., near the saddle points), we will have a useful approximation. If a fraction f_{block} of TST-crossing trajectories in the true ensemble are blocked from crossing in the biased-potential system due to $\Delta V_b(\mathbf{r})$ being nonzero along some portion of the dividing surface, the escape rate will be reduced by a factor no worse than $(1-f_{\text{block}})$. When the exact position of the dividing surface is known (e.g., for test systems), this effect can be quantified; in a TST-obeying system, the fraction of trajectories that will proceed unhindered is the ratio of partition functions for the biased and unbiased potentials, evaluated over the dividing surface,

$$1-f_{\text{block}}=\langle e^{-\beta \Delta V_b(\mathbf{r})}\rangle_{\delta_A}. \tag{17}$$

We will take the view that a definition for $\Delta V_b(\mathbf{r})$ can be found for which f_{block} is small, giving a good approximation to the exact long-time dynamics. Candidate definitions for $\Delta V_b(\mathbf{r})$ can be tested on systems with known dynamical properties. The examples presented below confirm that useful definitions for $\Delta V_b(\mathbf{r})$ exist, leading to substantial boost factors with negligible errors.

A possible definition for $\Delta V_b(\mathbf{r})$ suggested by Eq. (16) is the following:

$$\Delta V_b(\mathbf{r})=a\,\theta(\epsilon_1)(\epsilon_1)^2+c(\mathbf{C}_1\cdot\mathbf{g})^2, \tag{18}$$

where a and c are tunable parameters. The first term turns on smoothly as the lowest eigenvalue of $\mathbf{H}$ becomes positive, and is zero wherever the lowest eigenvalue is negative, due to the step function (here θ is the standard step function, not to be confused with Θ_A). The second term contributes wherever the slope along the lowest eigenvector is nonzero, regardless of the sign of the eigenvalue.

To perform MD requires the derivative of $\Delta V_b(\mathbf{r})$ with respect to each atom position. By analogy to the Hellman–Feynman forces, differentiating the first term in Eq. (18) in regions of positive ϵ_1 gives

$$\frac{\partial}{\partial x_i}[a\epsilon_1^2]=2a\,\frac{\partial}{\partial x_i}[\mathbf{C}_1^\dagger\mathbf{H}\mathbf{C}_1]=2a\mathbf{C}_1^\dagger\frac{\partial\mathbf{H}}{\partial x_i}\mathbf{C}_1, \tag{19}$$

where $\partial\mathbf{H}/\partial x_i$ is a matrix of third-derivatives of $V(r)$. Differentiation of the second term in Eq. (18) is not so straightforward, but a numerical approach can be designed that gives a good approximation, as described elsewhere.[36] The examples presented below utilize variations on the first term only.

A brief discussion of computational scaling is appropriate here. While in general, the work required to construct $\mathbf{H}$ scales as N^2, for a finite-ranged interatomic potential $\mathbf{H}$ becomes sparse as the system size increases beyond the cutoff range, so the actual scaling tends towards N for large systems. Similarly, performing a full diagonalization of $\mathbf{H}$ requires N^3 work, but iterative techniques such as the Lanczos method[37] can be used to find the lowest eigenvector with work scaling as N.

III. APPLICATIONS

A. Dynamics in a model potential

We first test and demonstrate the hyper-MD method for two model potentials on which exact dynamical results can be obtained for comparison. Although we know exactly where the minima and saddles are, we choose a bias potential that does not take advantage of this knowledge. We show that one can obtain the correct long-time dynamics with substantial boost factors.

We study a two-dimensional model potential of the form

$$V(x,y)=\cos(2\pi x)(1+d_1y)+\frac{d_2}{2}2\pi y^2 + d_3\cos(2\pi x/d_4). \tag{20}$$

This potential is periodic in the x direction and harmonic in the y direction. When $d_1=d_3=0$, the x period is unity, with equivalent minima ($V=-1$) at $x=k+\frac{1}{2}$, $y=0$, and saddles ($V=1$) at $x=k$, $y=0$, for all integer values of k. A positive value for the coupling coefficient d_1 lowers the energy of the saddles and minima by the same amount and shifts the minima in the $+y$ direction and the saddles in the $-y$ directions so that the diffusion path is not a straight line in x. This reduces the number of multiple-jump events. We initially choose $d_1=4$, $d_2=1$, and $d_3=0$, defining ''model potential I,'' which is shown in Fig. 2(a) and summarized in Table I.

For this low-dimensional system, coupling to a heat bath is essential for proper sampling from the canonical ensemble. We accomplish this via the Langevin equation.[38] For each configurational degree of freedom x_i ($x_i=x$ or y in this case),

$$\ddot{x}_i=\frac{1}{m}\frac{\partial V}{\partial x_i}-\alpha\dot{x}_i+\frac{A_i(t)}{m}, \tag{21}$$

where α is the friction coupling rate and $A_i(t)$ is the delta-correlated stochastic force which has zero mean and is related to α through the fluctuation-dissipation theorem,

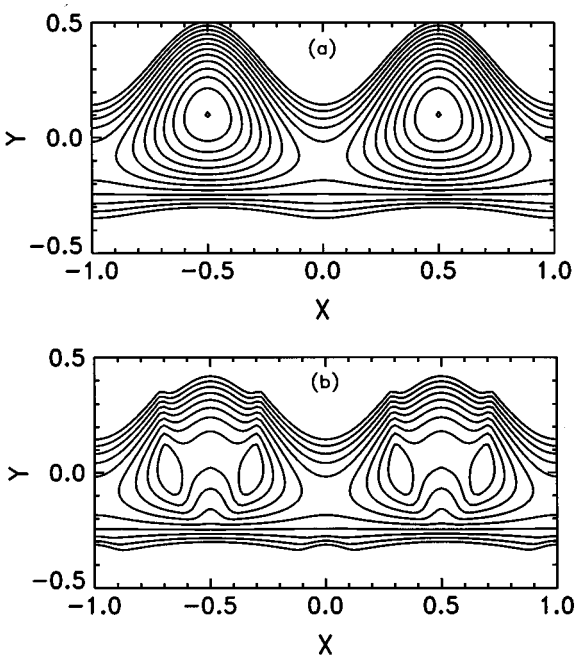

FIG. 2. Model potential I given by Eq. (20) with $d_1=4$, $d_2=1$, $d_3=0$. Two x periods are shown. The highest contour is at $V=2.0$ with a contour spacing of 0.25. (a) $V(x,y)$. (b) $V(x,y)+\Delta V_b(x,y)$, where ΔV_b is given by Eq. (31).

$$\int_{-\infty}^{\infty}A_i(t)A_j(t+\Delta t)dt=2\alpha mk_BT\delta(\Delta t)\delta_{ij}. \tag{22}$$

On time scales short relative to α^{-1}, the Langevin system obeys Newtonian dynamics, while on longer time scales the friction and stochastic driving force balance to give proper exploration of the canonical phase space at the chosen temperature. Proper integration of Eq. (21) is critical to obtain good stability and correct thermal properties with a reasonable time step. We used the Langevin–Verlet integration procedure described by Allen and Tildesley.[39] All calculations presented here employed $m=1$ and time steps of $\Delta t_{\mathrm{MD}}=0.02$ or 0.01. To obtain dynamical behavior representative of a realistic many-dimensional process such as surface or bulk diffusion, a value of $\alpha=0.5$ was chosen.[40] A higher value of α increases the number of friction-induced (i.e., Kramers[41]) recrossing events, in which the system is jostled back across the dividing surface before it clears the saddle region, while lower values of α result in a larger number of multiple-jump events, and bounce-back recrossing events.[42]

The one-dimensional diffusion constant is obtained from direct MD via the time evolution of the mean-squared displacement,

$$D=\frac{1}{2}\frac{d}{dt}\langle[x(t)-x(0)]^2\rangle, \tag{23}$$

which gives a value of $D=4.5\pm0.4\times10^{-5}$ at $k_BT=0.2$. At lower temperatures, where direct MD becomes more difficult (and ultimately unfeasible), the diffusion constant can be

TABLE I. Coordinates, energy, and Hessian eigenvalues (ϵ_1,ϵ_2) at the stationary points for the two model potentials based on Eq. (20). k is any integer, and the direction of the normal mode is given in parentheses after each eigenvalue. Numbering of the three minima for model potential II corresponds to Fig. 6.

	x	y	V	ϵ_1	ϵ_2
Model potential I ($d_1=4$, $d_2=1$, $d_3=0$)					
minimum	$k+0.5$	0.1013	−1.203	39.48(y)	55.48(x)
saddle	k	−0.1013	0.797	−23.48(x)	39.48(y)
Model potential II ($d_1=4$, $d_2=1$, $d_3=-0.75$, $d_4=3$)					
minimum 1	$3k+0.476$	0.100	−1.594	38.68(y)	57.26(x)
saddle 1→2	$3k+1.053$	−0.096	1.209	−26.00(x)	40.51(y)
minimum 2	$3k+1.500$	0.101	−0.453	39.48(y)	52.19(x)
saddle 2→3	$3k+1.947$	−0.096	1.209	−26.00(x)	40.51(y)
minimum 3	$3k+2.524$	0.100	−1.594	38.68(y)	57.26(x)
saddle 3→1	$3k+3.000$	−0.101	0.047	−20.19(x)	39.48(y)

computed using a combination of TST and the dynamical corrections method formulated for multistate systems.[8]

For the TST calculations, the $x=0$ line defines the dividing surface. Because the reduced mass of the reaction coordinate does not vary over the dividing surface, the momentum coordinates in Eq. (1) can be integrated analytically to give the mean one-dimensional speed, leaving only a configuration-space average to be computed,

$$k_{A\rightarrow}^{\mathrm{TST}}=(2k_BT/\pi m)^{1/2}\langle\delta_A(\mathbf{r})\rangle_A\,. \tag{24}$$

This average is evaluated using a MD implementation of the displacement-vector method,[43] an importance-sampling scheme ideally suited to this type of problem. These results are shown in column 2 of Table II. At $k_BT=0.2$, the TST rate for escape in both directions ($1.03\pm0.01\times10^{-4}$) agrees with the number of TST surface crossings per time from the direct-MD simulation ($1.01\pm0.04\times10^{-4}$), as it should.

Having chosen the TST dividing surface, the classically exact rate constants for the possible elementary events (single-jump, double jump, triple jump, etc.) are obtained using the dynamical corrections formalism, via trajectories initiated at the same dividing surface. The initial conditions for these saddle trajectories are sampled from a canonical ensemble within the TST plane (a line in this case), and assigned a Maxwellian-flux momentum distribution [$\mathrm{prob}(p_x)\propto|p_x|\exp(-\beta p_x^2/2m)$] perpendicular to the TST surface at $t=0$. After these trajectories have thermalized, i.e., after a time t exceeding the correlation time of the system, the elementary rate constant for a direct transition from state i to state j is computed from

$$k_{i\rightarrow j}^{\mathrm{el}}=k_{i\rightarrow}^{\mathrm{TST}}f_d(i\rightarrow j), \tag{25}$$

where the dynamical correction factor for the escape rate from state i is given by[8]

$$f_d(i\rightarrow j)=\frac{2}{N_{\mathrm{traj}}}\sum_{I=1}^{N_{\mathrm{traj}}}\gamma_I\Theta_j(I,t). \tag{26}$$

Here γ_I is the phase of trajectory I, which depends on whether the trajectory is initially exiting ($\gamma_I=+1$) or entering ($\gamma_I=-1$) state i. With perfect sampling (or, in this case, making use of symmetry), there is an equal number of trajectories with each phase. The state-occupation function, $\Theta_j(I,t)$, defined as in Eq. (3), acts as a filter to retain only those trajectories that are in state j at time t. In the infrequent-event regime, the rate constants from Eq. (25) are exact.

The diffusion constant can then be determined from the average squared jump length resulting from all the possible jumps (single-, double-,...) out of a representative state ($i=0$),

$$D=\tfrac{1}{2}\sum_j k_{0\rightarrow j}^{\mathrm{el}}l_{0j}^2, \tag{27}$$

where l_{0j} is the distance between sites 0 and j ($l_{0j}=|j|$ for this model potential). This expression for D, evaluated using half-trajectories, is exact even if the system is not in the infrequent-event regime[44] (i.e., even when the individual rate constants are not valid[45]).

TABLE II. TST and dynamical corrections results for model potential I. The TST rates are summed over both escape directions; each dynamical correction factor, $f_d(i\rightarrow\pm j)$, is summed over both left and right j-long jump events [i.e., $f_d(0\rightarrow\pm j)=f_d(0\rightarrow j)+f_d(0\rightarrow -j)$]. Each f_d was computed from 10^4 trajectories using Eq. (26) with $t=10$. Numbers in parentheses indicate one-standard-deviation uncertainty in the last digit.

k_BT	k^{TST}	$f_d(0\rightarrow\pm1)$	$f_d(0\rightarrow\pm2)$	$f_d(0\rightarrow\pm3)$	D/D^{TST}
0.20	$1.03(1)\times10^{-4}$	0.771	0.024	0.002	0.88(1)
0.15	$3.72(4)\times10^{-6}$	0.855	0.009	0.0	0.897(7)
0.10	$4.83(8)\times10^{-9}$	0.917	0.002	0.001	0.926(4)
0.09	$5.12(10)\times10^{-10}$	0.928	0.001	0.0	0.930(3)

The dynamical correction factors obtained for this potential are shown in Table II, along with the overall diffusion correction factor, D/D^{TST}, where the TST diffusion constant is defined by assuming uncorrelated single hops at the TST rate,

$$D^{\mathrm{TST}}=\tfrac{1}{2}k_{0\rightarrow}^{\mathrm{TST}}l_{01}^{2}. \tag{28}$$

This becomes $D^{\mathrm{TST}}=k^{\mathrm{TST}}/2$ in the present case. As the temperature is lowered, the general trend is towards fewer multiple jump events and fewer bounce-back recrossing events, so that TST becomes an increasingly good approximation. At very low temperatures, D/D^{TST} levels off at a value dictated by the friction-induced recrossings, which are temperature independent. For example, at $k_BT=0.01$, $D/D^{\mathrm{TST}}=f_d(0\rightarrow\pm1)=0.951$. This is in excellent agreement with the prediction from a one-dimensional Kramers model ($f_d=0.950$) based simply on the ratio of the friction coefficient to the angular frequency of the unstable mode at the saddle[46] ($\alpha/\omega_c=0.103$).

It is also instructive to consider the full-harmonic approximation to TST, using the Vineyard expression,[12]

$$k^{\mathrm{HTST}}=n_{\mathrm{path}}\frac{\Pi_i^{n_{\mathrm{dim}}}\nu_i^{\mathrm{min}}}{\Pi_i^{n_{\mathrm{dim}}-1}\nu_i^{\mathrm{sad}}}\exp(-E_a/k_BT), \tag{29}$$

where E_a is the static barrier height, $\{\nu_i^{\mathrm{min}}\}$ are the n_{dim} normal mode frequencies at the minimum, $\{\nu_i^{\mathrm{sad}}\}$ are the $n_{\mathrm{dim}}-1$ nonimaginary normal mode frequencies at the saddle point ($\nu_i=\epsilon_i^{1/2}/2\pi$), n_{path} is the number of escape paths (2 here), and n_{dim} is the number of dimensions (2 here). Assuming uncorrelated jumps, the full harmonic approximation to the diffusion constant is thus

$$D^{\mathrm{HTST}}=\tfrac{1}{2}k^{\mathrm{HTST}}l^{2}, \tag{30}$$

In the present model, $l=1$, $E_a=2.0$ and the preexponential frequency is 2×1.185.

We now examine the diffusion using hyper-MD. For simplicity, we define a bias potential that is nonzero only where the lowest Hessian eigenvalue is positive, using a modified version of the first term in Eq. (18),

$$\Delta V_b(x,y)=\frac{z}{1+z/z_{\mathrm{max}}};\quad z=a\,\theta(\epsilon_1)\epsilon_1^2. \tag{31}$$

Here z_{max} limits the maximum size of ΔV_b, in turn controlling the size of the exponential in Eq. (12). Values of $a=0.004$ and $z_{\mathrm{max}}=1.5$ were chosen with very little experimentation. The biased potential is shown as a contour plot in Fig. 2(b). Figure 3 shows a projection of the minimum-energy pathway for this potential (V minimized with respect to y for each fixed value of x) for both the unbiased and biased form. It is easy to see that, as desired, this bias potential does not affect the potential in the immediate vicinity of the saddle point. However, comparison of Figs. 2(a) and 2(b) indicates that the TST dividing surface (defined as the $x=0$ line) is corrupted in the region near $y=-0.3$ This is an example of the possibility discussed in Sec. II B, in which a fraction f_{block} of reactive trajectories will be unable to cross the dividing surface when the bias is turned on. Evaluation of Eq. (17) from a simulation restricted to the TST surface gives $1-f_{\mathrm{block}}=0.998\pm0.001$ at $k_BT=0.2$, and $1-f_{\mathrm{block}}=1.0000$ at $k_BT=0.1$, so the fraction of hindered trajectories is negligible in this case.

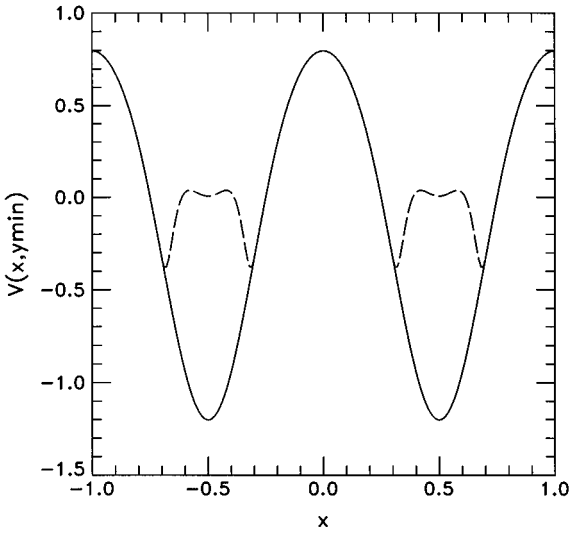

FIG. 3. Minimum-energy path (potential minimum along y for each x position) for model potential I. The solid line is V and the dashed line is $V+\Delta V_b$.

The hyper-MD results are summarized in the first five columns of Table III. We first consider the prediction of the TST escape rate. The derivation of Eq. (9) guarantees that the TST crossing rate will be correct in the hyperdynamics, provided that the sampling is complete and $f_{\mathrm{block}}=0$. Comparing the crossing rate from the hyper-MD run (column four in Table III) with the TST rates in Table II shows agreement within statistical uncertainty at all temperatures. This indi-

TABLE III. Hyper-MD runs, showing raw total MD run time (t_{MD}), observed average boost factor, dividing-surface crossing rate (n_{cross}/t_b), and diffusion constant from the slope of the mean-square displacement ($D^{\mathrm{hyper-MD}}$). Also shown for comparison are values of D obtained from full TST (D^{TST}), and TST plus dynamical corrections ($D^{\mathrm{TST+dyncor}}$), based on the data in Table II. Numbers in parentheses indicate one-standard-deviation uncertainty in the last digit.

k_BT	t_{MD}	boost	n_{cross}/t_b	$D^{\mathrm{hyper-MD}}$	D^{TST}	$D^{\mathrm{TST+dyncor}}$
0.20	2.5×10^{5}	46.7	$1.03(3)\times10^{-4}$	$5.1(4)\times10^{-5}$	$5.15(5)\times10^{-5}$	$4.53(7)\times10^{-5}$
0.15	5.0×10^{6}	200.1	$3.78(7)\times10^{-6}$	$1.8(1)\times10^{-6}$	$1.86(2)\times10^{-6}$	$1.67(2)\times10^{-6}$
0.10	1.0×10^{8}	3435.	$4.8(1)\times10^{-9}$	$2.4(1)\times10^{-9}$	$2.41(4)\times10^{-9}$	$2.24(4)\times10^{-9}$
0.09	1.0×10^{8}	8682.	$5.3(2)\times10^{-10}$	$2.5(4)\times10^{-10}$	$2.56(5)\times10^{-10}$	$2.38(5)\times10^{-10}$

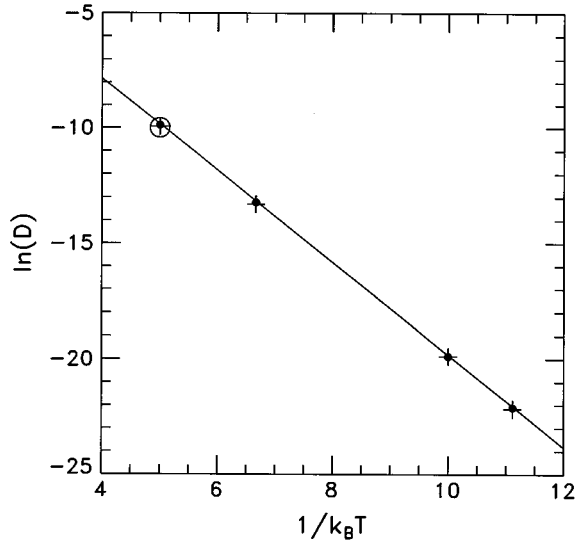

FIG. 4. Arrhenius plot of the diffusion coefficients for model potential I, showing a comparison of $D^{\text{direct-MD}}$ (○), $D^{\text{hyper-MD}}$ (●), and $D^{\text{TST+dyncor}}$(+). The symbols are sized for clarity. The line is the full harmonic TST approximation [Eqs. (29 and (30)], and is indistinguishable from a least-square line through the D^{TST} points (not shown).

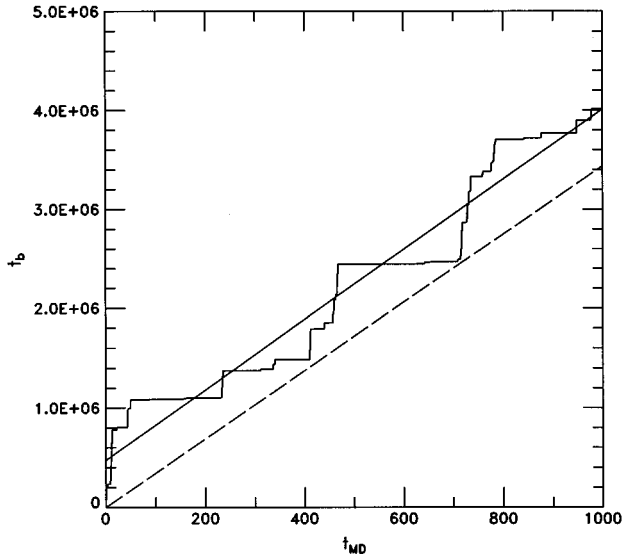

FIG. 5. Evolution of the boosted time, shown for a small segment of the hyper-MD run on model potential I at $k_BT=0.1$. The slope of the least-squares fit to the points (solid line) gives an estimate of the boost for this time interval, already in good agreement with the boost averaged over the whole run (shown by the slope of the dashed line).

cates that the hyper-MD simulations have been run long enough to achieve an accurate estimate of the total boosted time, t_b. The small subwells introduced by the bias potential due to its rapid onset as ϵ_1 grows (at $x=-0.68$, $y=0.0$, and $x=-0.32$, $y=0$) apparently cause no problem.

We now focus on D, a physical observable independent of the dividing surface, representative of the type of property that might be sought in a real application. At all temperatures, there is good agreement (within the error bars) between $D^{\text{hyper-MD}}$ and D^{TST}. At the highest temperature ($k_bT=0.2$), $D^{\text{hyper-MD}}$ is ~13% higher than the exact diffusion constant $D^{\text{TST+dyncor}}$, probably due to the disruption of the recrossing events by ΔV_b. This agreement improves as the temperature is lowered. We conclude that the correlated dynamical activity causes no unexpected errors in $D^{\text{hyper-MD}}$. The diffusion constants are plotted in Arrhenius form in Fig. 4, along with a line representing the full-harmonic prediction from Eqs. (29) and (30), which is seen to be a good approximation.

As the temperature is lowered, the average boost factor increases due to its exponential dependence on inverse temperature, a general characteristic of this method. At the lowest temperature studied here ($k_BT=0.09$), the boost factor is 8.68×10^3. For this potential, computing the higher derivatives requires a factor of 3 times more computational work for each hyper-MD step than for a direct-MD step, so the net computational gain is 2.9×10^3. Even at this high boost value, the simulation is stable. A comparable direct-MD simulation at this temperature would be impractical, requiring 4.3×10^{13} MD steps. In general, very rough, terms, if the bias potential reduces the well depth by a factor of q ($q\sim2$ here), then a hyper-MD simulation will be feasible at a temperature q times lower than for direct MD, not counting the extra computational work of computing $\Delta V_b(\mathbf{r})$.

Figure 5 shows the nonlinear evolution of the boosted time at $k_BT=0.1$. As the system passes through regions of large ΔV_b, t_b increases rapidly; this behavior alternates with periods of almost no progress as the system explores regions where $\Delta V_b\simeq0$. In this case, relatively long low-boost intervals occur while the system is caught in the one of the local minima created by the bias potential. The interval shown is a small fraction (10^{-5}) of the total simulation time, although a reasonable estimate of the average boost ratio is already forming.

We now turn to model potential II, which is summarized in Table I and shown in Fig. 6. This potential has two types of binding sites; for one of the binding sites the two escape paths have very different barriers. The dynamical behavior of this system is characterized by two time scales, as can be seen in the time evolution of the mean-squared displacement in Fig. 7. The initial, large slope is due to the rapid jumps between the two binding sites (minima 1 and 3 in Table I) separated by a low barrier of 1.641. To execute long-range diffusion requires surmounting a much larger barrier (2.803) to get to the next low-energy, double-well set, corresponding to an effective jump length of 3.

Figure 8 shows an Arrhenius plot of the diffusion constants from hyper-MD simulations. At $k_BT=0.2$ and $k_BT=0.25$, there is excellent agreement with the direct-MD simulations. At $k_BT=0.3$, there are substantially more bounce-back recrossings in the direct MD than in the hyper-MD, reducing D.

For simplicity, we estimate the correct diffusion constant at the lower temperatures using harmonic TST within an uncorrelated-jump model. Because there is more than one type of binding site, no simple, closed-form expression such as Eq. (30) exists. Instead, kinetic Monte Carlo is employed,

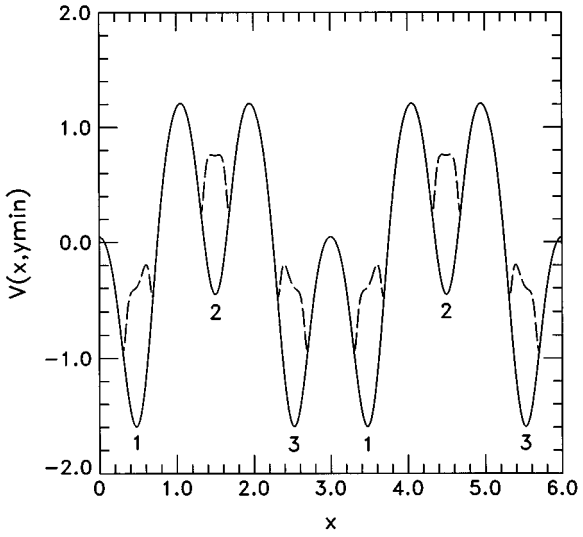

FIG. 6. Minimum-energy path (potential minimum along y for each x position) for model potential II, showing two periods. The dashed line is $V+\Delta V_b$.

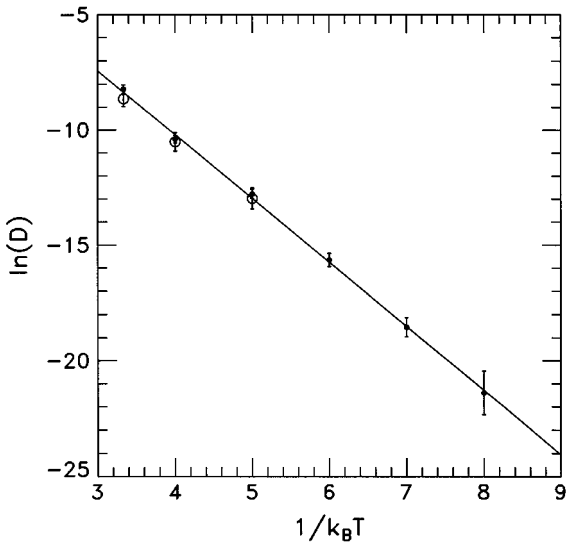

FIG. 8. Arrhenius plot of diffusion coefficients for model potential II, showing direct MD (○) and hyper-MD (●). The line is a least-squares fit to the Vineyard-based kinetic Monte Carlo results (the points are omitted for clarity).

using the six Vineyard rates[47] as the entries in the rate catalog.[18] Over the temperature range shown, the kinetic Monte Carlo points fall on a straight line with slope -2.77 and intercept 0.88. The long-time dynamics picture described above, in which escape over the highest barrier leads to a hop length of three, predicts a slope of -2.803 and intercept of 0.973 (i.e., the log of the preexponential factor), in good agreement. The hyper-MD diffusion constants are seen to fall on this line. At the lowest temperature ($k_BT=0.125$), the average boost factor is 358.

Although the boost factors for model potential II were similar to those observed for model potential I at a given temperature, much longer runs were required to obtain good statistics for the diffusion constant, because a higher barrier (2.803 rather than 2.0) dictated the long-time dynamics. This illustrates the point that for a system with multiple barrier heights, the available boost is controlled by the lowest barrier in the system. This can be seen graphically in Fig. 6. If the bias potential is increased until it represents a significant fraction (e.g., more than half) of the height of the larger barrier, the lower barrier at $x=3$ becomes more of a local minimum than a barrier. In such a situation, the TST assumption (that there are no recrossing events) breaks down, as the system simply vibrates back and forth across the $x=3$ dividing surface. This situation can be prevented by choosing the bias potential according to the height of the lowest barrier. (In a many-dimensional system, allowing the bias potential to go higher than a certain barrier need not cause any problems, provided there are paths available for the system to circumnavigate the peak in $V+\Delta V_b$.) On the other hand, if one knows in advance that transitions over the lowest barrier are unimportant to the long-time dynamical properties of interest (a judgement that should be made with some care), choosing an aggressive bias potential that leads to correlated transitions over the lowest barrier may offer a way to achieve more boost.

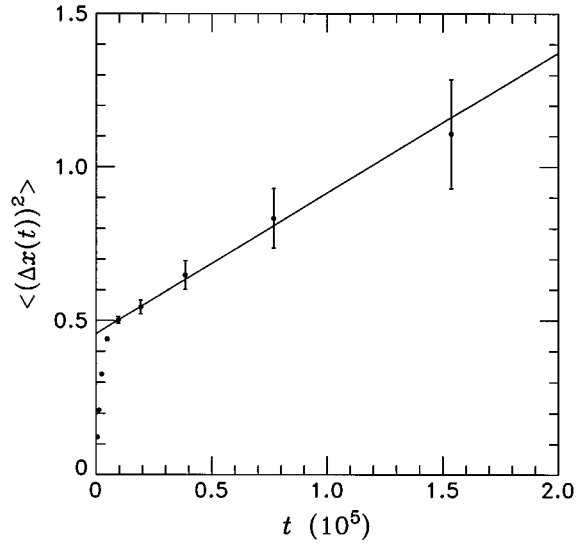

FIG. 7. Mean-squared displacement from direct-MD run at $k_BT=0.2$ on model potential II.

B. Ni adatom diffusion on a Ni(100) terrace

To demonstrate the method in a more realistic application, we now examine the diffusive motion of a Ni adatom on a Ni(100) terrace at $T=500$ K using an embedded atom method (EAM) interatomic potential. As shown in Fig. 9, the narrow terrace confines the motion of the adatom to hops in the $+x$ or $-x$ directions (no constraint prohibits hops off the terrace in the y direction other than a much higher barrier). Nine atoms (the adatom and the top layer of the substrate) out of 37 total are allowed to move in the simulation. This system is designed to give realistic motion of a diffusing

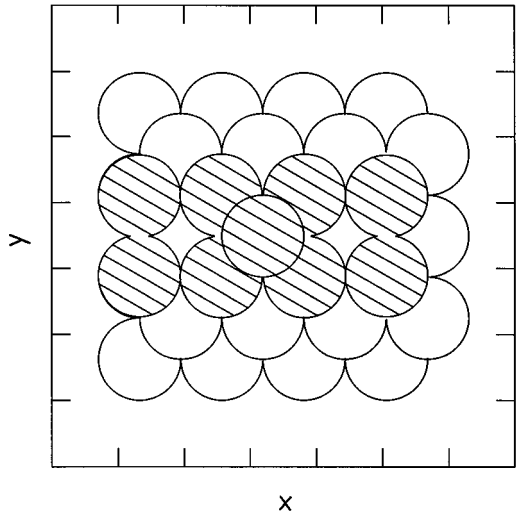

FIG. 9. Surface-normal view of Ni adatom on single-channel Ni(100) terrace. One x period (4 binding sites) is shown, with tick marks 2 Å apart. The 9 shaded atoms (adatom and first layer of substrate) are free to move in the simulation.

adatom with a minimal number of degrees of freedom so that direct construction and diagonalization of the Hessian (scaling as N^3) is not computationally prohibitive. As mentioned above, more sophisticated approaches exist for reducing this scaling to N.

The simulation cell is periodic in x and has free boundaries in y and z. The Ni lattice is expanded to the quasiharmonic-predicted lattice constant at $T=500$ K ($3.520 \times 1.0084 = 3.550$ Å). As for the model potentials, a Langevin procedure is used to thermostat the system, with $\alpha = 2.0\times10^{12}$ s^{-1} and a time step of $\Delta t_{\mathrm{MD}} = 3.0\times10^{-15}$ s. (For comparison, the normal mode frequencies $\{\nu_i^{\min}\}$ range from 3.0×10^{12} s^{-1} to 9.2×10^{12} s^{-1}.)

The EAM potential is a semiempirical form[48] that augments a pair potential with a local, density-dependent term. As discussed elsewhere,[49,50] this form of potential has had considerable success in describing fcc transition metals. The Ni potential we use here[51] was fit to the bulk lattice constant, cohesive energy, elastic constants, and unrelaxed vacancy formation energy, and the bond length and bond energy of the gas-phase diatomic molecule. This potential predicts surface diffusion barriers in very good agreement with field ion microscope experiments for Ni(100) and a number of other Ni surfaces.[52]

We first discuss estimates of the exact rate constant for diffusive motion on this terrace. At $T=500$ K, direct MD is prohibitive, so we compute the classically exact rate constant using TST augmented by dynamical corrections, as we did for model potential I. Taking the saddle plane ($3N-1=26$ dimensions) as the TST surface, the TST rate constant was computed from Eq. (24) using the displacement-vector method,[43] giving $k^{\mathrm{TST}} = 5.04\pm0.10\times10^5$ s^{-1} (total escape rate summed over both directions). Dynamical-corrections trajectories, initiated at this same dividing surface, were evolved for a time of 2.0 ps, exceeding the correlation time. The final resting position of these 1000 trajectories initiated at the boundary between states 0 and 1 (953 in state 1, 46 in state 0, 1 in state -1) were used as described above[8] to compute dynamical correction factors of $f_d(0\rightarrow\pm1) = 0.91 \pm 0.01$ and $f_d(0\rightarrow\pm2) = 0.0\pm0.001$. The overall rate constant is thus $4.6\pm0.1\times10^5$ s^{-1}, corresponding to an escape time of 2.18 ± 0.05 μs.

Using the Vineyard approach, we obtain a static barrier of 0.744 eV and a pre-exponential factor of 8.11×10^{12} s^{-1} [Eq. (29) with $n_{\mathrm{dim}}=3N=27$, and $n_{\mathrm{path}}=2$]. At $T=500$ K, $k^{\mathrm{HTST}} = 5.14\times10^5$ s^{-1}. The full harmonic treatment is thus an excellent approximation to the exact TST value and is within 7% of the full dynamical rate constant.[53]

We now turn to the hyper-MD simulation. As in the last section, we use a bias potential based on the first term in Eq. (18). The bias term is nonzero whenever ϵ_1 exceeds a base value, ϵ_{base}; i.e.,

$$\Delta V_b(\mathbf{r}) = a\,\theta(\epsilon_1-\epsilon_{\mathrm{base}})(\epsilon_1-\epsilon_{\mathrm{base}})^2. \tag{32}$$

Choosing a negative value for ϵ_{base} increases the overall boost, at the risk of having a nonzero $\Delta V_b(\mathbf{r})$ somewhere on the dividing surface. Knowing $\epsilon_1 = -1.57$ eV/Å^2 at the saddle point in this system, we chose $\epsilon_{\mathrm{base}} = -1.4$ eV/Å^2 and $a=0.05$ Å^4/eV. Using Eq. (17) in a simulation restricted to the saddle plane gave $1-f_{\mathrm{block}} = 0.96\pm0.01$. For this demonstration calculation, we have made use of our knowledge of the system to increase the boost. For comparison, using $\epsilon_{\mathrm{base}}=0$ eV/Å^2 and $a=0.20$ Å^4/eV gives a boost factor of 40 ± 5, about ten times lower than the boost factor achieved here. In real applications, where the saddle points are not predetermined, a more conservative approach would be safer, to prevent accidentally blocking a saddle point with a lower imaginary frequency. For those cases, a more sophisticated form for $\Delta V_b(\mathbf{r})$, utilizing both the eigenvalue and the eigenvector-projected gradient, can be used to increase the boost.[36] This is especially important for larger systems, because the fraction of configuration space with all positive Hessian eigenvalues decreases as the number of degrees of freedom increases.

Calculation of third derivatives of the EAM potential, apparently required by Eq. (19), can be avoided. The second derivative of the potential along an arbitrary direction, **s**, can be approximated numerically by

$$\frac{\partial^2 V(\mathbf{r})}{\partial \mathbf{s}^2} \cong \frac{V(\mathbf{r}+\eta\mathbf{s}) + V(\mathbf{r}-\eta\mathbf{s}) - 2V(\mathbf{r})}{\eta^2}, \tag{33}$$

where η is a small number. After diagonalizing the Hessian, the exact lowest eigenvalue (ϵ_1) is replaced by its approximation via Eq. (33) ($\epsilon_1^{\mathrm{num}}$), by using the lowest eigenvector as **s**. Differentiating Eq. (33) gives

$$\frac{\partial \epsilon_1^{\mathrm{num}}}{\partial \mathbf{r}} = \frac{\partial}{\partial \mathbf{r}}\left[\frac{\partial^2 V(\mathbf{r})}{\partial \mathbf{s}^2}\right]_{\mathbf{s}=\mathbf{C}_1} = \frac{\mathbf{g}(\mathbf{r}+\eta\mathbf{C}_1) + \mathbf{g}(\mathbf{r}-\eta\mathbf{C}_1) - 2\mathbf{g}(\mathbf{r})}{\eta^2}, \tag{34}$$

an approximation that depends only on the gradient of V at three points.

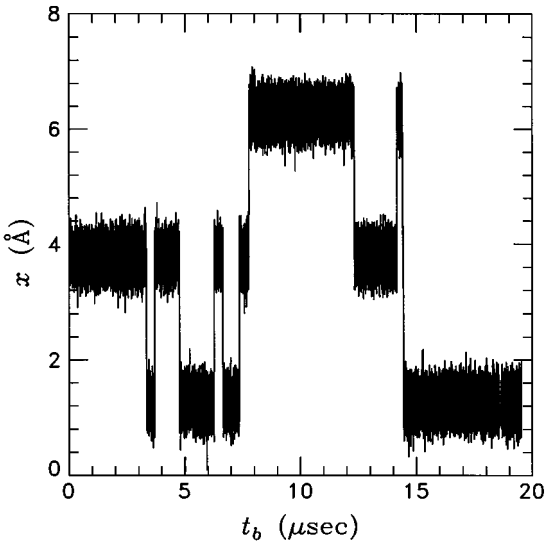

FIG. 10. Ni adatom x position vs boosted time for diffusion on the Ni(100) terrace shown in Fig. 9, at $T=500$ K.

Figure 10 shows the time evolution of the x position of the adatom during a hyper-MD simulation for 1.5×10^7 steps. The position was stored every 500 steps. The time (t_b) between points in the figure thus varies (e.g., causing the gap at $t_b=18.6$ μs) due to fluctuations in the instantaneous boost factor, which is 434 ± 5 on average. Also, any brief excursions that quickly recrossed (within 1.5 ps of MD time) would not show up in this plot, and were not monitored. At 14.41 μs, there are two independent jumps in the same direction separated by 73.5 ps of MD time (i.e., this is not a double jump). From the 11 jumps that occurred, the escape time is estimated as $\tau_{\rm esc}=1.8\pm0.5$ μs, in statistical agreement with the exact value. Averaging with a second, equivalent simulation, which yielded 7 jumps in 19.597 μs, gives $\tau_{\rm esc}=2.2$ μs. This 20-μs simulation took only a few days of CPU time on a modern scalar workstation. Each integration step took $\sim$6 times more work than in a direct-MD simulation, for a net computational gain of $434/6=72$ over direct MD.

IV. CONCLUSIONS

Although the dynamics of infrequent-event systems can be understood within a TST framework, application of TST to these systems is often hindered due to incomplete knowledge of the states through which the system will evolve. The alternative has been to use direct MD, but the time scale is limited to nanoseconds or less. We have shown that with the proper choice of bias potential [$\Delta V_b(\mathbf{r})$], one can transform the problem into one where time is no longer an independent variable, but, rather, evolves nonlinearly at an accelerated pace and can be estimated statistically. This hyper-MD method is exact if TST holds, and if the bias potential is zero at all TST dividing surfaces and does not block access to any escape paths or otherwise trap the trajectory. We have shown that bias potentials can be constructed from properties of the Hessian which meet these requirements to a good approximation and that, indeed, highly accurate accelerated dynamics result. This simple form based on the lowest Hessian eigenvalue probably would not be sufficient for gas-phase systems with centrifugal barriers that move the optimum TST dividing surface away from the potential energy saddle,[54] nor for liquids, which often have negative eigenvalues irrelevant to the reaction coordinate of interest. This hyper-MD method works in continuous space, like direct MD, rather than mapping atom positions onto a lattice. Consequently, it does not suffer the danger of lattice-based kinetic Monte Carlo methods, in which states that are not easily mapped onto a lattice (e.g., if they have disordered character) are left out of the simulation, leading to erroneous dynamics. (On the other hand, if all the states can be enumerated, and the rates between them calculated, kinetic Monte Carlo is substantially faster than hyper-MD.)

For the model potentials investigated, boost factors greater than 10^3 were achieved, and the known correlated dynamical activity (e.g., bounce-back recrossings, and multiple jumps) had a minor or negligible impact on the quality of the predicted diffusion constants.

Applying the method to a more realistic process, the diffusion of a Ni adatom on a narrow Ni(100) terrace using an EAM interatomic potential, a boost factor of 434 was obtained, giving a total run time of almost 20 μs. For this demonstration case, $\Delta V_b(\mathbf{r})$ was constructed with some advanced knowledge of the saddle point properties, but more sophisticated forms for $\Delta V_b(\mathbf{r})$ [e.g., utilizing the eigenvector-projected gradient as in the second term of Eq. (18)] should offer comparable or even greater boosts with complete generality.

Future development of the method looks promising, with room for improvement in the forms for $\Delta V_b(\mathbf{r})$ and efficiency of the computational implementation. For example, the method may be parallelizable even for small system sizes, something that is difficult in normal MD simulations. Extensions to quantum dynamics may also be possible, via the Feynman-path-centroid formulation of quantum transition state theory.[55]

ACKNOWLEDGMENTS

The author gratefully acknowledges stimulating and helpful discussions with Joel Kress, Richard L. Martin, Tom Lenosky, Brad Holian, and Frances Houle, and critical comments on the manuscript from Tony Redondo, Joel Kress, Paul Davids, and Lawrence Pratt. This work was supported by the Laboratory-Directed Research and Development (LDRD) program at Los Alamos National Laboratory.

[1] R. Marcelin, Ann. Phys. **3**, 120 (1915).
[2] E. Wigner, Z. Phys. Chem. B **19**, 203 (1932).
[3] H. Eyring, J. Chem. Phys. **3**, 107 (1935).
[4] J. Horiuti, Bull. Chem. Soc. Jpn. **13**, 210 (1938).
[5] D. G. Truhlar and B. C. Garrett, Acc. Chem. Res. **13**, 440 (1980).
[6] P. Hanggi, P. Talkner, and M. Borkovec, Rev. Mod. Phys. **62**, 251 (1990).
[7] D. Chandler, J. Chem. Phys. **68**, 2959 (1978); J. A. Montgomery, Jr., D. Chandler, and B. J. Berne, *ibid*. **70**, 4056 (1979).
[8] A. F. Voter and J. D. Doll, J. Chem. Phys. **82**, 80 (1985).

[9] For an excellent review of dynamical corrections to TST, see J. B. Anderson, Adv. Chem. Phys. **91**, 381 (1995).
[10] J. C. Keck, Discuss. Faraday Soc. **33**, 173 (1962).
[11] C. H. Bennett, in *Diffusion in Solids: Recent Developments*, edited by J. J. Burton and A. S. Nowick (Academic, New York, 1975), p. 73.
[12] G. H. Vineyard, J. Phys. Chem. Solids **3**, 121 (1957).
[13] R. E. Kunz and R. S. Berry, J. Chem. Phys. **103**, 1904 (1995).
[14] P. J. Feibelman, Phys. Rev. Lett. **65**, 729 (1990).
[15] G. L. Kellogg and P. J. Feibelman, Phys. Rev. Lett. **64**, 3143 (1990).
[16] C. Chen and T. T. Tsong, Phys. Rev. Lett. **64**, 3147 (1990).
[17] M. Villarba and H. Jónsson, Phys. Rev. B **49**, 2208 (1994).
[18] A. F. Voter, Phys. Rev. B **34**, 6819 (1986).
[19] J. T. Hynes, in *The Theory of Chemical Reaction Dynamics*, edited by M. Baer (Chemical Rubber, Boca Raton, 1985), Vol. IV, p. 171.
[20] N. Grønbech-Jensen and S. Doniach, J. Comp. Chem. **15**, 997 (1994).
[21] A. M. Mathiowetz, A. Jain, N. Karasawa, and W. A. Goddard, Proteins-Structure Function and Genetics **20**, 227 (1994).
[22] G. A. Huber and S. Kim, Biophys. J. **70**, 97 (1996).
[23] P. V. Kumar, J. S. Raut, S. J. Warakomski, and K. A. Fichthorn, J. Chem. Phys. **105**, 686 (1996).
[24] M. E. Tuckerman, G. J. Martyna, and B. J. Berne, J. Chem. Phys. **93**, 1287 (1990).
[25] J. D. Doll, J. Chem. Phys. **73**, 2760 (1980).
[26] E. A. Carter, G. Ciccotti, J. T. Hynes, and R. Kapral, Chem. Phys. Lett. **156**, 472 (1989).
[27] J. P. Valleau and S. G. Whittington, in *Modern Theoretical Chemistry*, edited by B. J. Berne (Plenum, New York, 1977), Vol. 5, p. 137.
[28] J. P. Valleau and G. M. Torrie, in *Modern Theoretical Chemistry*, edited by B. J. Berne (Plenum, New York, 1977), Vol. 5, p. 169.
[29] C. H. Bennett, in *Algorithms for Chemical Computation*, edited by R. E̊. Christofferson (American Chemical Society, Washington, D.C. 1977), p. 63.
[30] B. J. Berne, M. Borkovec, and J. E. Straub, J. Phys. Chem. **92**, 3711 (1988).
[31] A. F. Voter and J. D. Doll, J. Chem. Phys. **80**, 5814 (1984).
[32] This trajectory should be coupled to a heat bath, at least weakly, to provide proper canonical, rather than microcanonical, behavior.
[33] The reflecting barrier is for this thought experiment only; in applications of the hyperdynamics method, no such barriers are constructed.
[34] E. M. Sevick, A. T. Bell, and D. N. Theodorou, J. Chem. Phys. **98**, 3196 (1993).
[35] M. Toller, G. Jacucci, G. DeLorenzi, and C. P. Flynn, Phys. Rev. B **32**, 2082 (1985).
[36] A. F. Voter (unpublished).
[37] B. N. Parlett, *The Symmetric Eigenvalue Problem* (Prentice–Hall, Englewood Cliffs, 1980).
[38] S. Chandrasekhar, Rev. Mod. Phys. **15**, 1 (1943).
[39] M. P. Allen and D. J. Tildesley, *Computer Simulation of Liquids* (Oxford, New York, 1987), p. 263, Eq. (9.24).
[40] With this value of α, the dynamics are well into the underdamped regime; the angular normal mode frequencies at the minimum are 6.28 and 7.45.
[41] H. A. Kramers, Physica **7**, 284 (1940).
[42] For example, in the direct-MD simulation at $k_BT=0.2$, examination of the successive crossing times showed 34 friction-induced recrossings events (subsided by $t=1$), 95 bounce-back recrossing events (some of these on the second and third vibration), and 35 forward multiple jump events, all subsided by $t=5$, out of a total of 1011 TST-surface crossings with an average escape time of $\tau_{\rm esc}=9090$.
[43] A. F. Voter, J. Chem. Phys. **82**, 1890 (1985).
[44] A. F. Voter, Phys. Rev. Lett. **63**, 167 (1989).
[45] A. F. Voter, J. D. Doll, and J. M. Cohen, J. Chem. Phys. **90**, 2045 (1989).
[46] S. Chandrasekhar, Rev. Mod. Phys. **15**, 1 (1943), Eq. (507).
[47] Alternatively, D could be computed exactly for this potential using TST and dynamical corrections for each of the saddle planes, so that the kinetic Monte Carlo simulation would be based on the correct rate constants for each type of escape event (single jump to left, single jump to right, double jump to left, etc.) out of each unique minimum.
[48] M. S. Daw and M. I. Baskes, Phys. Rev. B **29**, 6443 (1984).
[49] A. F. Voter, in *Intermetallic Compounds: Principles and Practice*, edited by J. H. Westbrook and R. L. Fleischer (Wiley, New York, 1995), Vol. 1, p. 77.
[50] M. S. Daw, S. M. Foiles, and M. I. Baskes, Mater. Sci. Rep. **9**, 251 (1993).
[51] A. F. Voter and S. P. Chen. Mater. Res. Soc. Symp. Proc. **82**, 175 (1987).
[52] C. L. Liu, J. M. Cohen, J. B. Adams, and A. F. Voter, Surf. Sci. **253**, 334 (1991).
[53] A commonly used approximation to the full harmonic treatment, in which the frequency factor is replaced by the frequency of the vibrational mode at the minimum corresponding to motion towards the saddle point (when such a mode can be uniquely identified), is not as accurate. The x-direction frequency of the adatom with all other atoms held fixed (4.79×10^{12} s^{-1}) is 41% lower than the Vineyard frequency. The frequency of the x_1-predominant eigenmode of the full 27-dimensional system (3.16×10^{12} s^{-1}) is 61% low.
[54] M. J. Davis and R. T. Skodje, in *Advances in Classical Trajectory Methods*, (JAI, New York, 1992), Vol. I, p. 77.
[55] M. J. Gillan, J. Phys. C **20**, 3621 (1987); G. A. Voth, D. Chandler, and W. H. Miller, J. Chem. Phys. **91**, 7749 (1989); G. K. Schenter, M. Messina, and B. C. Garrett, *ibid*. **99**, 1674 (1993).